

Fluctuations induced transition of localization of granular objects caused by degrees of crowding



Soutaro Oda^a, Yoshitsugu Kubo^b, Chwen-Yang Shew^{c,d,*}, Kenichi Yoshikawa^a

^a Faculty of Life and Medical Sciences, Doshisha University, Kyotanabe 610-0394, Japan

^b Department of Physics, Kyoto University, Kyoto, 606-8502, Japan

^c Ph.D. Program in Chemistry, The Graduate Center of the City University of New York, New York, NY 10016, USA

^d Department of Chemistry, College of Staten Island, Staten Island, NY 10314, USA

HIGHLIGHTS

- Confined large and multiple small granular particles are studied under vibration.
- At higher densities, large particles shift from cavity boundary to cavity interior.
- This universal behavior is induced by the size disparity of the mixture.
- A simple entropic model is developed to elucidate experimental observations.

ARTICLE INFO

Article history:

Received 17 November 2015

Accepted 27 June 2016

Available online 4 July 2016

Keywords:

Non-equilibrium
Granular particles
Modeling
Fluctuation

ABSTRACT

Fluctuations are ubiquitous in both microscopic and macroscopic systems, and an investigation of confined particles under fluctuations is relevant to how living cells on the earth maintain their lives. Inspired by biological cells, we conduct the experiment through a very simple fluctuating system containing one or several large spherical granular particles and multiple smaller ones confined in a cylindrical dish under vertical vibration. We find a universal behavior that large particles preferentially locate in cavity interior due to the fact that large particles are depleted from the cavity wall by small spheres under vertical vibration in the actual experiment. This universal behavior can be understood from the standpoint of entropy.

© 2016 The Authors. Published by Elsevier B.V.

This is an open access article under the CC BY-NC-ND license (<http://creativecommons.org/licenses/by-nc-nd/4.0/>).

1. Introduction

Fluctuations are present almost ubiquitously in both macroscopic and microscopic systems. How does external fluctuation lead to the emergence of a stable pattern? This is still a large target in the research of modern physics, including astronomy, fluidic systems, living matters, etc. Industrially, it has been a common practice to use fluctuations as a way to facilitate packing of grains, foods, and pharmaceutical powders at macroscopic scale, for example [1,2]. In nature, biological cells at microscopic scale are under constant thermal and external fluctuations, and life activities are regulated within confined and crowded cells with 20%–40% (w/w) of polymeric species [3,4]. The nucleus is a prominent organelle in the length scale of a highly crowded eukaryotic cell,

and its location is commonly observed in the interior of a biologic cell away from the boundary of cellular membranes. A similar structural feature is found in a cellular nucleus. Within a crowded nucleus, a dense sphere-like nucleolus, consisting of RNA and proteins, forms a significantly recognizable structure during the interphase of a cell cycle [5], which also tends to situate in the inner nuclear region away from membranes.

In fact, the above picture that large organelles distribute away from the confined membrane is somehow counter-intuitive. According to the entropic depletion force effect suggested by Asakura and Oosawa, [6], the large particle such as nucleus in cells or nucleolus in nuclei should preferentially localize next to the confined boundary, that is, membranes. One may argue that the complex nature inside a cell or a nucleus may induce some enthalpic energies to surpass entropic effect. However, within the highly crowded cell or nucleus, excluded volume interactions remain a crucial component [7] to regulate their heterogeneous structure. The entropic contribution deserves a detailed examination [3,8–10].

* Corresponding author.

E-mail address: chwenyang.shew@csi.cuny.edu (C.-Y. Shew).

Here, we conduct an experiment by using the binary mixture of rigid granular particles confined on a 2D cylindrical disk, a system driven by cellular materials and environment, where large and small particles represent large organelles and crowders, respectively. Fluctuations are introduced by incorporating vertical vibration to induce constant collisions among particles similar to thermal motion in liquid.

Besides the biological point of view, our experiment renders an opportunity to examine the structure of the rigid granular particles in a dissipative system. Under vibration, granular particles gain energy, but the energy of each particle is dissipated to the environment due to frictions. It has been pointed out by Komatsu and Tanaka that such a dissipative system is far from equilibrium in nature, and energy dissipation determines the state selection [11]. The immediate question to be addressed is: after our system under vibration reaches a steady state, what physical state should be present with size-disparity granular particles. The next question is how the steady state in our experimental result should be analyzed.

This manuscript is organized as follows. An overview of our experimental system is first given, and then experiment results are presented followed by model studies based on entropic argument for data analysis. Monte Carlo simulation is summarized in the Appendix A.

2. Experimental system

Motivated by biological cells and 2D granular systems, we elucidate the interplay between excluded volume interaction and fluctuation for confined particles via a “real-life” experiment by mixing N_L large spherical granular particles of diameter d_L with N_S smaller ones of diameter d_S confined in a cylindrical dish of diameter D . In analogy with a cell, the large sphere mimics the large organelle in a cell or in a nucleus, and small spheres model other smaller cellular substances as crowders. All the interparticle and particle–wall interactions are at the level of excluded volume interaction. In our experiment, d_L is fixed at 10 mm and D is chosen to be 60 mm. The confined mixture is then subject to regular vertical vibration, similar to the work by Pacheco-Vazquez et al. [12]. The vertical vibration can be partly viewed as a greatly simplified way to model non-uniform fluctuations around cellular membranes, in which some area of cellular membranes undergoes more fluctuation than others, such as matter exchange or membrane undulation.

The experimental system is shown in Fig. 1(a) and (b). We set vibration frequency $f = 120$ Hz and amplitude $A = 55$ μm that produce enough acceleration to bounce granular particles up from the dish surface. Note that our conclusion is insensitive to the choice of f and A . This vibration force first induces frequent collisions among granular particles like the thermal motion of cellular particles. Also, the vibration motion actually triggers an additional degree of freedom for the vertical translational motion of confined particles. To quantify the crowding level in a simple manner, we define “packing fraction” as the projected area of the large and small spheres onto the cavity surface, given by $\eta = (N_S d_S^2 + N_L d_L^2)/D^2$. Despite its near two-dimensional nature, this experiment provides the major components like those in a confined cell or nucleus, and enables us to systematically investigate various effects that switch the large sphere from the confined boundary to the interior of the cavity based on excluded volume interaction. Our experiment covers a wide density range of granular particles from $\eta = 0.1$ to 0.66 (dilute to high density state). In the high density state, our experiment is also suitable to test the Brazil nut effect in which the large sphere shifts to the top of the granular mixture under vibration [13–16]. A distinct difference between the Brazil nut effect and our experiment is that

we place spheres on the same surface, which may be viewed as a single-layer granular particles. In addition, there is no significant effect due to gravitational force in our results, which is essentially important in Brazil nut effect.

3. Experimental results

The real-time experimental trajectory of the large sphere is obtained with long movies. Fig. 1 shows the typical snapshots at time $t = 0$ and 540 s (left panel) and the trajectory of the large sphere (right panel) for two distinct packing fractions $\eta = 0.1$ (with $N_S = 29$) in (c) and 0.6 (with $N_S = 229$) in (d) for $N_L = 1$, and the case of $N_L = 3$ (with $N_S = 229$) for $\eta = 0.66$ up to $t = 40$ s in (e), when $d_L : d_S = 10 : 3$. Note that the dotted circles in the trajectory plots indicate the outermost boundary within the disk which the center of mass of a large sphere can reach. For the lower η , the large sphere preferentially distributes around the cavity boundary. Whereas, for the higher η , the large sphere switches its preferential location to the inner cavity. For $N_L = 3$, we observe essentially the same trend as $N_L = 1$ in which large spheres preferentially distribute near the inner cavity at higher crowding levels. It is clear that this is general behavior for large spheres switching their preferential location from confined boundary to cavity interior under the vibration experiment for sufficiently crowded condition. In the following, our study will be focused on the case of $N_L = 1$ to reveal the physics behind this universal behavior.

The trajectories shown in Fig. 1 are transformed into the spatial density distribution function of the large sphere ρ_L by dividing the circular disk into 6 layers. ρ_L is then determined via the histogram of the large sphere located in each layer divided by the area of a given layer. The thus obtained ρ_L allows us to quantify the preferential localization of the large sphere for each condition. The interplay between η and d_S on the structure of the confined large sphere is systematically studied from ρ_L in such a way that d_L and D are fixed, but d_S and N_S are varied. Fig. 2 plots the phase diagram to summarize the specific localization of the large sphere as a function of η and the size ratio d_L/d_S in (a) as well as the typical density distribution function for $\eta = 0.1, 0.2$, and 0.6 when $d_L : d_S = 10 : 3$ in (b), corresponding to the three points ((i), (ii), and (iii)) highlighted in Fig. 2(a) with boxes. In the phase diagram, the preferential localization of the large sphere can be divided into three categories: (1) near the cavity boundary (denoted by \circ); (2) near the cavity boundary and the inner region of the cavity (denoted by \bullet); (3) in the inner region of the cavity (denoted by \bullet). Also, the dashed line in Fig. 2(a) is the phase boundary predicted by a theoretical model to be discussed in the context of Fig. 4, in which the large sphere distributes near equally around cavity boundary and inner cavity (denoted by \circ in Fig. 2(a)). Fig. 2(a) indicates that as η and/or d_L/d_S ratio (reduction of the size of small spheres) are increased, the large sphere tends to localize in the inner cavity. By decreasing the size of small spheres, it enhances migration of the large sphere towards the inner cavity, and such a finding agrees with the literature result that smaller crowders promote crowding effect [7].

The three categories of specific localization of the large sphere are further illustrated in Fig. 2(b). For the low packing fraction ($\eta = 0.1$) in Fig. 2(b), the large particle exhibits a significantly high probability around the cavity wall, which is consistent with the entropic depletion effect suggested by Asakura and Oosawa [6]. As η is increased to 0.2, the large sphere exhibits a similar probability to distribute near the cavity boundary and the inner cavity. For $\eta = 0.6$, the large sphere distributes away from the cavity wall, and has a high spatial density near the central region of the cavity. This result coincides with the common picture that the nucleus and

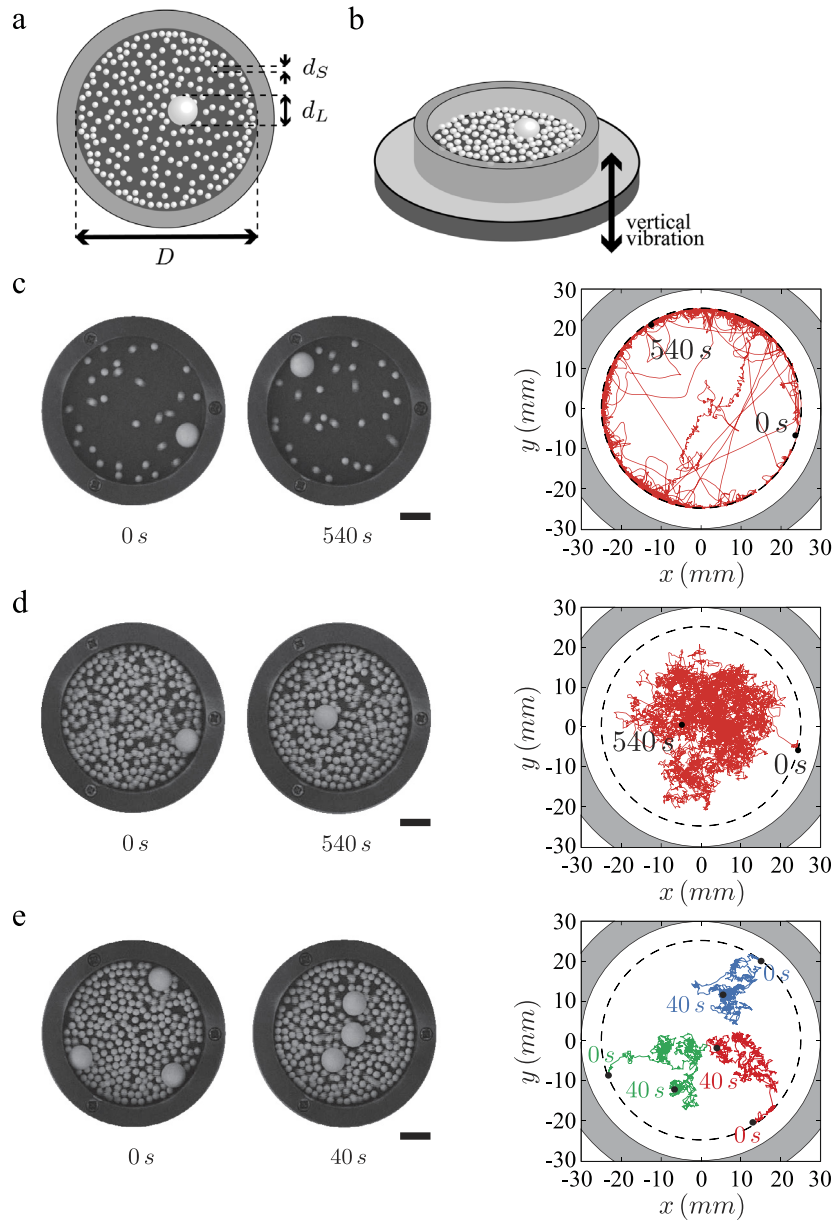


Fig. 1. Schematic representations of the experimental system with bird view in (a) and side view in (b); typical snapshots at 0 and 540 s (left panel) and the real-time trajectories of the large sphere (right panel) for two distinct packing fractions $\eta = 0.1$ ($N_L = 1$ and $N_S = 29$) in (c) and 0.6 ($N_L = 1$ and $N_S = 229$) in (d), and the case of $N_L = 3$ and $N_S = 229$ for $\eta = 0.66$ up to $t = 40$ s in (e), where $d_L = 10$ mm, $d_S = 3$ mm and $D = 60$ mm. The scale bar is 10 mm. Note that the dotted circles in the trajectory plots indicate the outermost boundary which can be reached by the center of mass of a large sphere within the cylindrical disk.

the nucleolus situate in the region away from the membrane of a biological cell and a nucleus, respectively.

The dynamic origin of the switching process in our experiment is tested by analyzing the kinetic energy ratio before and after a sphere colliding with the cavity wall by using a high speed camera that generates 500 frames/s. Fig. 3 plots the mean kinetic energy ratio of a particle with η before and after it bounces from the cavity wall for a large sphere (denoted by \bullet) and a small sphere (denoted by \circ) when $d_L : d_S = 10 : 3$ in (a), and a series of snapshots (extracted from the video clip in the supplementary material, Appendix B) and schematic explanation of our observation at $\eta = 0.6$ in (b). At the low $\eta (= 0.1)$, the mean kinetic energy ratio is around unity for both large and small spheres. As η increases, the mean kinetic energy ratio of the large sphere increases and exceeds that of a small sphere at around $\eta = 0.18$. At high η , the large sphere has a relatively higher kinetic energy gain after bouncing from the area of the wall compared to a small sphere. Above $\eta =$

0.3, the kinetic energy ratio becomes leveled off for both large and small spheres.

The snapshots in Fig. 3(b) show that at a high crowding level, the large sphere is lifted to the top of small spheres, and moves inwards to the inner cavity. The starting point of this lifting process occurs when the large sphere is near the cavity wall. As illustrated in Fig. 3(b), the large sphere experiences frequent collisions from small spheres. When the large sphere is near the wall, the vertical motion of small spheres generated by vibration in the experiment imposes a lifting force on the large sphere to raise it to the top of small spheres. The collision energy transferred from small spheres to the large sphere enhances the kinetic energy of the large sphere when it bounces from the area near the wall. Whereas, for a small sphere, the kinetic energy may dissipate quickly and evenly to surrounding spheres and the cavity wall. The friction from the cavity wall is a possible energy dissipation pathway to slow down small spheres near the boundary. As a result, these spheres

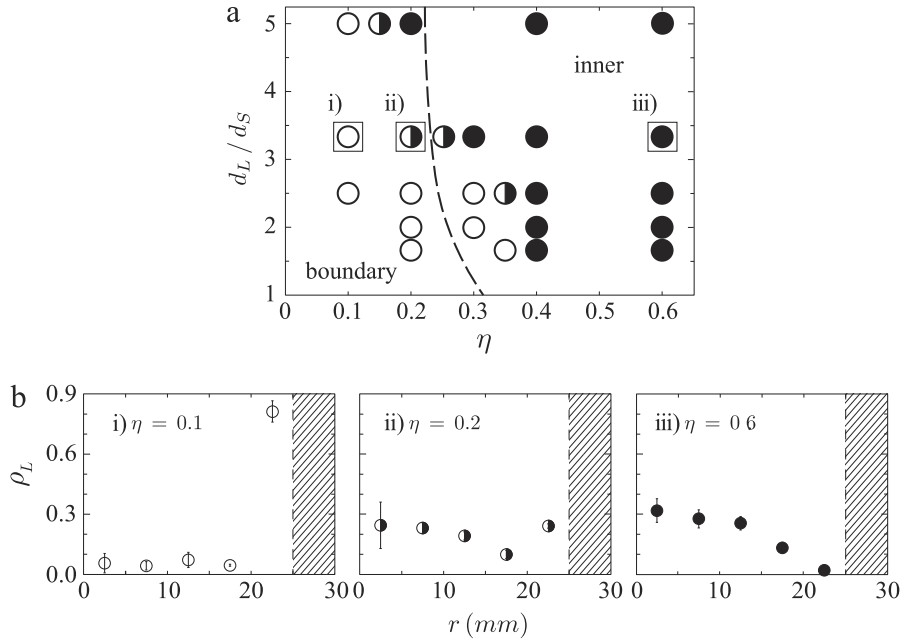


Fig. 2. Experimental phase diagram for specific localization of the large sphere as a function of packing fraction η and the size ratio d_L/d_S in (a), and the typical density distribution function of the large sphere ρ_L for three different packing fractions $\eta = 0.1, 0.2,$ and 0.6 when $d_L : d_S = 10 : 3$ in (b) with error bars, corresponding to the three points ((i), (ii), and (iii)) highlighted in (a) with boxes. The dashed line in (a) is the approximate boundary to divide the preferential localization of the large sphere predicted by a theoretical model to be discussed in the context of Fig. 4. Note that the half-filled circles \bullet denote the regime of the experimental phase boundary where the large sphere preferentially distributes both near the wall and the interior of the cavity.

around the wall act just like that they are under depletion forces. Moreover, our experiment represents the single-layer granular particles, and our observation of the large sphere “floating” above small spheres is consistent with the spontaneous segregation on the Brazil nut effect [13–15]. Within a finite cavity, our experiment suggests a general trend in the single layer Brazil nut effect that can be initiated from the cavity boundary.

4. Model studies

The vibration experiment creates a dissipative system in which energy gained by granular particles is dissipated into heat due to friction forces on the surface of the disk. Nevertheless, the small fluctuating system of our experiment quickly reaches a steady state, and the thus obtained density distribution functions become time-independent. Since the granular particles in our experiment are rigid, it is instructive to elucidate our findings by considering the athermal hard sphere model dominated by entropy, prior to more complex dynamic studies.

In the vibration experiment, the large sphere is basically “desorbed” from the cavity wall, and the entropy of small spheres on the two-dimensional surface becomes crucial to understand the structure of confined particles under crowding condition even with vertical vibration. These arguments are consistent with our Monte Carlo simulation results based on the hard sphere model in the Appendix A in the following fashion. First, the large particle is excluded from the cavity wall under crowding and vertical fluctuation (to account for extra degrees of freedom due to vibration). Secondly, the simulated density distribution function of small particles displays only a secondary change after the vertical fluctuation is incorporated. The 2D configurational entropy of small spheres (due to free space) becomes a reasonable order parameter to study the preferential location of the large sphere. The packing fraction defined in this work based on the 2D projected area of individual spheres onto the cavity surface play the essential role for our study of the above 2D order parameter.

Experimentally, the cavity wall may have two major impacts on structure: (1) it induces depletion forces on spheres, and (2) it is an additional energy dissipation pathway to dissipate energy of a particle in our non-equilibrium system, both of which can act like attractive forces and may be enhanced for small spheres at higher densities. To model these possible collective forces, we introduced an entropic two-state model phenomenologically. For lower particle densities, the cavity wall induces weak adsorption on particles, and this model (Model A) imposes no adsorption on particles (i.e., more fluctuation allowed for a particle near wall), whereas at higher densities, an adsorption layer is introduced to Model B and the number of adsorbed particles depends on particle densities. Model A allows the large sphere to be around the cavity wall, but Model B impedes the large sphere to access the region of cavity boundary. The fundamental question lies in how to determine the characteristic density to discern low density regime from high density regime. Such a distinction is insightful to elucidate the preferential location of the large sphere, that is, the large sphere prefers to be near wall at lower densities and away from wall at higher densities. At near η_{crit} , the large sphere displays similar probability in the cavity interior and the cavity wall, as shown in Fig. 2(b).

The entropic expression of Model A with small spheres that are fully “desorb” from the cavity wall and experience no depletion forces near the wall takes the following form.

$$S_A \sim k_B N_S \ln \frac{\frac{\pi}{4} D^2 - \pi N_S d_S^2}{N_S} \quad (1)$$

where k_B is the Boltzmann constant. While small spheres are adsorbed to the surface due to the depletion force from the wall, the entropy is modified to the following form (S_B) with N_w small spheres adsorbed to the wall. In Model (B) with small spheres that are under depletion force from the wall, and are partially “adsorbed” onto the cavity wall, its entropy reads

$$S_B \sim k_B (N_S - N_w) \ln \frac{\frac{\pi}{4} D^2 - \pi N_S d_S^2 + \alpha N_w}{N_S - N_w} \quad (2)$$

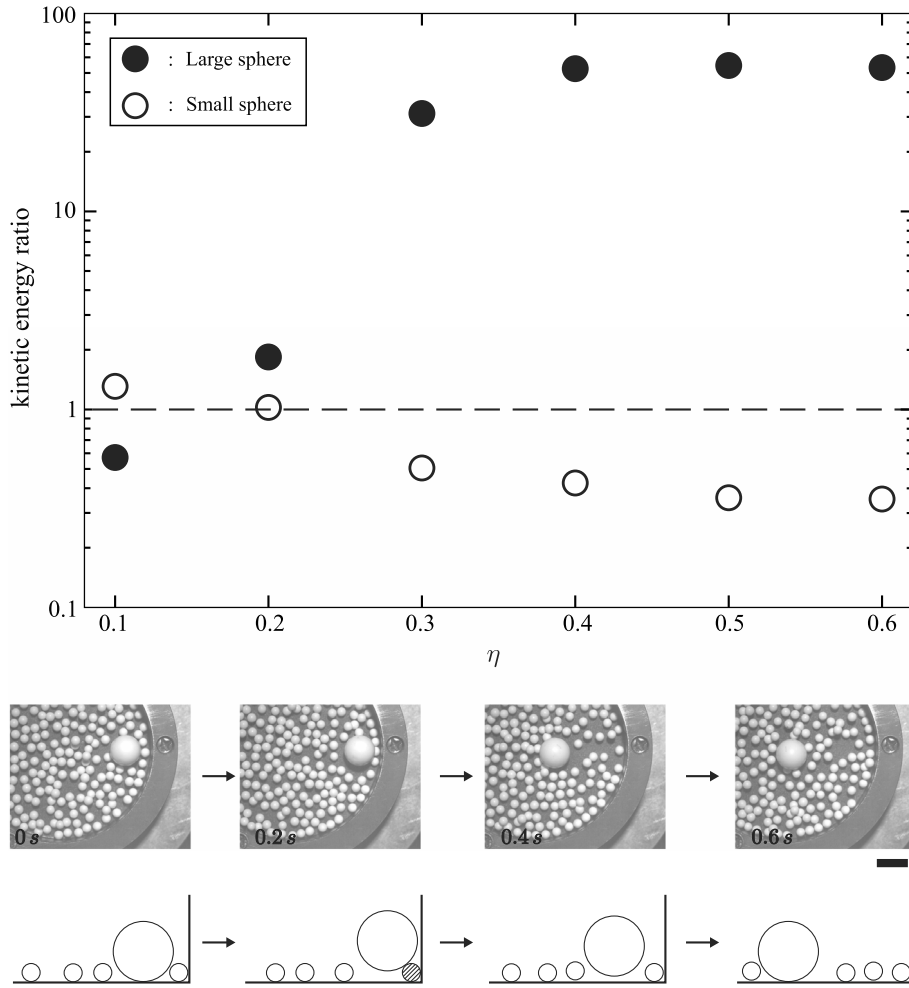


Fig. 3. Comparison of the mean kinetic energy ratio of a particle before and after bouncing from the cavity wall for a large sphere (denoted by ●) and a small sphere (denoted by ○) with different packing fractions when $d_L : d_S = 10 : 3$ in (a), and snapshots and schematic explanation for our observation at $\eta = 0.6$ in (b). The scale bar is 10 mm.

where α is to account for the difference between the excluded volume of a particle away from the wall and of a particle next to the cavity wall, which reads

$$\alpha = 2r^2\theta - \frac{1}{2}\{R^2\varphi - \sqrt{[R^2 + (2r)^2 + (R-r)^2]^2 - 2[R^4 + (2r)^4 + (R-r)^4]}\} \quad (3)$$

where $\varphi = 2\cos^{-1}\{[R^2 + (R-r)^2 - (2r)^2]/2R(R-r)\}$; $\theta = \cos^{-1}(1 - x^2/8r^2)$; $x = \sqrt{2R^2(1 - \cos\varphi)}$; $R = D/2$; $r = d_S/2$. The approximation in Model B is that the particles not adsorbed onto the cavity wall have the excluded volume identical to those particles in Model A. The optimal N_w to maximize S_B for a given N_S is obtained from $dS_B/dN_w = 0$. Note that the “depletion force” in Model (B) captures the possible energy dissipation pathway in our vibration experiment in which small spheres are driven towards the cavity wall because the friction from the cavity wall. Even though the large sphere is not explicitly incorporated in our model, our analysis provides a useful viewpoint as a way of elucidating the possibility to place a large sphere around the boundary of the cavity (or to exclude the large sphere from the boundary) due to its size disparity while small spheres are in equilibrium. This picture is consistent with the experimental process in that all the spheres are under spatial fluctuation induced by vibration, and the large sphere tends to find a location not frequently disturbed by fluctuating small spheres, which is sensitive to the crowding level

of the system. The relative kinetics between the large sphere and small spheres is, thus, indirectly embedded in the model study.

In our analysis, we suggest that characteristic density (corresponding to the density that leads to η_{crit}) should be at the point when these two models exhibit the same entropy. It indicates that both models have identical statistical weight at this condition. Furthermore, for densities below η_{crit} , the entropy of Model A is lower than that of Model B, the attractive forces from wall are weak for small spheres, and vice versa for densities above η_{crit} .

We first plot the calculated entropy of the two models as a function of η , and illustrate how the crossing packing fraction (i.e., characteristic density) η_{crit} is determined. Note that η is directly proportional to N_S . Fig. 4(a) compares the entropy of the two models against packing fraction η for the case $D : d_S = 60 : 3$. The crossover between S_A and S_B occurs at around the crossing packing fraction $\eta_{crit} = 0.22$. After the packing fraction η exceeds η_{crit} , S_B becomes greater than S_A (thick solid line in Fig. 4(a)) because the adsorbed spheres create sufficient free space for the rest of spheres away from the wall. In a separate calculation, we have further explored how the number of adsorbed particles in Model B depends on the total particle number (or density), and the results are shown in Fig. 4(b) and (c). Fig. 4(b) compares the number of small spheres adsorbed onto the wall N_w for a series of N_S between model calculations, denoted by the line, and experimental measurement, denoted by symbols with error bars. Without any fitting parameter, the calculated N_w surprisingly agree well with our experimental

measurement in a near quantitative fashion in Fig. 4(b). This result shows that the simple model based on entropic argument captures the essential physics of our experiment. Fig. 4(c) displays the same plot as in Fig. 4(b) in which the schematics of possible configuration for a few selected N_S are plotted. Note that η_{crit} obtained from Fig. 4(a) is also included in Fig. 4(c) for comparison. When N_S is small, N_w is basically equal to zero since the system entropy is maintained by random distribution of small spheres. As N_S is increased, N_w rises linearly, and becomes leveled off for the large enough N_S due to the saturation of adsorbed spheres on the cavity wall. Based on the above two models, the crossing packing fraction η_{crit} in Fig. 4(a) is corresponding to the N_S value in the middle of the straight line as N_w increases from zero to its saturation value. Fig. 4(d) and (e), respectively, plot the predicted crossing packing fraction η_{crit} as a function of the size of small spheres when the dish diameter $D = 60$ mm and as a function of the dish diameter when $d_S = 3$ mm. The model predicts that η_{crit} increases as the size of small spheres increases in Fig. 4(d). Namely, the small spheres with a smaller size exhibits a greater effect on the entropy change in Model (B). Meanwhile, in Fig. 4(e), the model predicts that η_{crit} is less sensitive to D compared to the effect of the size of crowdors. As shown in Fig. 2(a), without any fitting parameter, the calculated η_{crit} , denoted by dashed line, is consistent with the experimental phase boundary, denoted by \bullet . Such a result indicates that the two-dimensional packing entropy of confined small spheres sustains migration of the large sphere from the region near the cavity wall to the interior of the cavity. With the vertical fluctuation, the large sphere has little contribution to packing entropy because under crowded condition, it detaches from the cavity wall and gains entropy by moving itself on the top of small spheres, as shown in Fig. 3.

One may speculate that the granular systems should behave differently from the usual physicochemical systems such as homogeneous gases and liquids composed of a large number of small molecules. In the present study, we have examined the validity on the simple model with entropy argument, which is under stationary fluctuation with the expectation that granule particles may fluctuate over the entire phase space consisting of a great number of positional and motional degrees of freedom. As a result, we have obtained essentially the same behavior on the specific localization of the large sphere in Figs. 2(a) and 4(b).

Alternatively, it is a tempting approach to interpret the experimental trend, based on the numerical model following the framework of fluid dynamics. Consequently, one can argue the specific localization of the large sphere from the aspect of (repulsive) hydrodynamic interactions, HIs [17], by which the depletion attraction between the large sphere and the cavity wall is weakened. In the present study, we have found an interesting phenomenon on the switching of the localization of a large sphere. In order to interpret the observed experimental trend, we have adapted the simple argument on the evaluation of entropy. As mentioned above, such a framework of theoretical consideration provides a clear physical picture into our observation. The problem to adapt HIs is that, for the experimental conditions with a relatively small number of spheres as in our case, the model with HIs becomes unreliable. It may be interesting, in a near future, to combine the theoretical arguments between the simple model in this work and the current fluidic modeling.

Furthermore, in the present study, we take into account of the fluctuating behavior of spheres with the size larger than 1 mm. Such consideration seems to be against the current argument on the modeling of Brazil-nut effect. The difference on the effect of fluctuation is attributable to the difference in the main factor to cause the “segregation”. In Brazil-nut effect, gravity is essential and the effect of gravity becomes negligible for smaller particles less than 1 mm. Whereas, the segregation of the present experiment, gravitational effect is minimum. Instead, collision between particles and also with the wall play the main role as the thermal motion in liquid state.

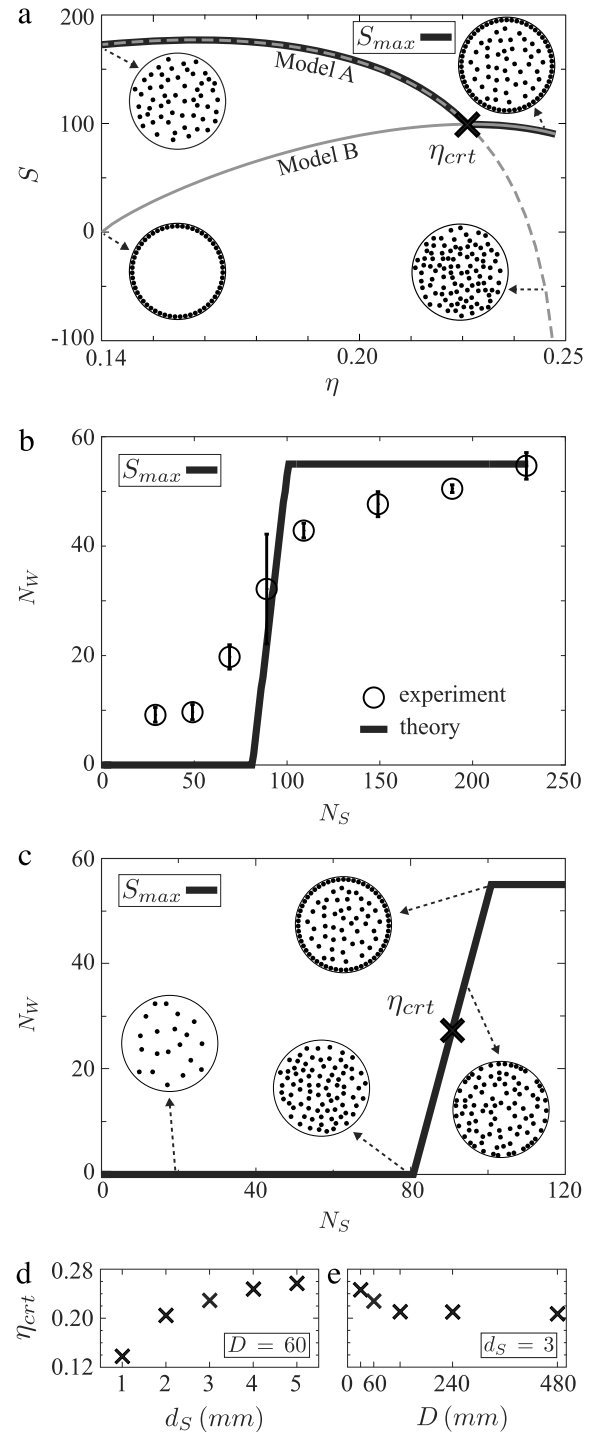


Fig. 4. Comparison of the calculated entropy of the two models against packing fraction η when $D : d_S = 60 : 3$ in (a); the corresponding number of small spheres N_w adsorbed onto the cavity wall from (a) a function of N_S in (b) and (c); the predicted crossover packing fraction η_{crit} from Model (B) against d_S when $D = 60$ mm and against D when $d_S = 3$ mm in (d) and in (e), respectively. In (b), we compare model calculation, denoted by the line with the experiment measurement, denoted by symbols with error bars.

5. Conclusions

We conduct the experiment through a very simple fluctuating system containing one or several large spherical granular particles and multiple smaller ones confined on a cylindrical dish under vertical vibration. We find a universal behavior emerges for the steady state, that is, large particles preferentially locate in cavity interior due to the fact that large particles are depleted from the

cavity wall by small spheres under vertical vibration in the actual experiment. This universal behavior can be understood from the standpoint of 2D configurational entropy. To further improve our quantitative understanding, our future work aims at elucidation of energy dissipation mechanisms in our experimental system. For theoretical analysis, a possible scheme is to introduce an effective interaction between spheres and the cavity wall into our current model. Further, a systematic study is awaited to investigate how such an interaction depends on particle density, particle size and vibration frequency.

Acknowledgments

This work was supported by JSPS KAKENHI Grant Number 15H02121 and 25103012. CYS thanks the partial support from the City University of New York PSC grants (Nos. 67134-0045 and 68108-0046) and from the JSPS Invitation Award (No. S12033).

Appendix A. Monte Carlo simulation

In contrast to the picture of a two-dimensional liquid, an additional degree of freedom is present in our experiment through vertical vibration, that is, the translational motion perpendicular to the dish surface. We investigate its qualitative effect on the structure of mixture by using Monte Carlo simulation for two models: (1) 2D model: a two-dimensional liquid consisting of one large sphere of diameter d_L and 60 small spheres of diameter d_S ($=0.3d_L$) confined in a circular surface of diameter D of various sizes. All the interactions are considered at the level of excluded volume interaction including the wall–particle interaction. The interaction potential between particles is given by

$$\begin{aligned} \frac{V(r_{ij})}{k_B T} &= 0 \quad \text{if } r > r_{ij}^c \\ &= \infty \quad \text{if } r \leq r_{ij}^c \end{aligned} \quad (4)$$

where k_B and T are the Boltzmann constant and temperature, respectively; r_{ij} is the distance between particle i and particle j ; r_{ij}^c is the nearest distance between two particles where $r_{SS}^c = d_S$ between two smaller spheres and $r_{LS}^c = \sqrt{d_L d_S}$ between a large and a small sphere on the 2D dish surface. The particle–wall interaction potential reads

$$\begin{aligned} \frac{V_{i,\text{wall}}(r)}{k_B T} &= \infty \quad \text{if } r > (D - d_i)/2 \\ &= 0 \quad \text{if } r \leq (D - d_i)/2 \end{aligned} \quad (5)$$

where r is the radial distance on the two-dimensional circular surface, d_i is the diameter of particle i where $d_i = d_L$ and d_S for the large sphere and small spheres, respectively. (2) Quasi-2D model: small spheres and the large sphere randomly fluctuate along the z -direction in the range $0.15-0.3d_L$ and $0.5-0.7d_L$, respectively. This allows small spheres to move up a half of its diameter and the large sphere to reach the top of small spheres roughly within the range of the average altitude of small spheres. In the interaction potential of Eq. (4), r_{ij}^c is adjusted to $(d_L + d_S)/2$. In the simulation, the density distribution function per particle is calculated by dividing the circular disk into 60 layers. One may expect that in a living cell, fluctuations are far more complex than the quasi-two-dimension hard sphere liquid here [18]. Nevertheless, this greatly simplified model is the starting point to reveal the effect of the additional vertical fluctuation, as opposed to the 2D model, on the structure of the mixture of rigid spheres.

Fig. A.1 compares the simulated density distribution function of the large sphere of the two-dimensional liquid (2D model), denoted by solid symbols, with that of the quasi-two-dimensional

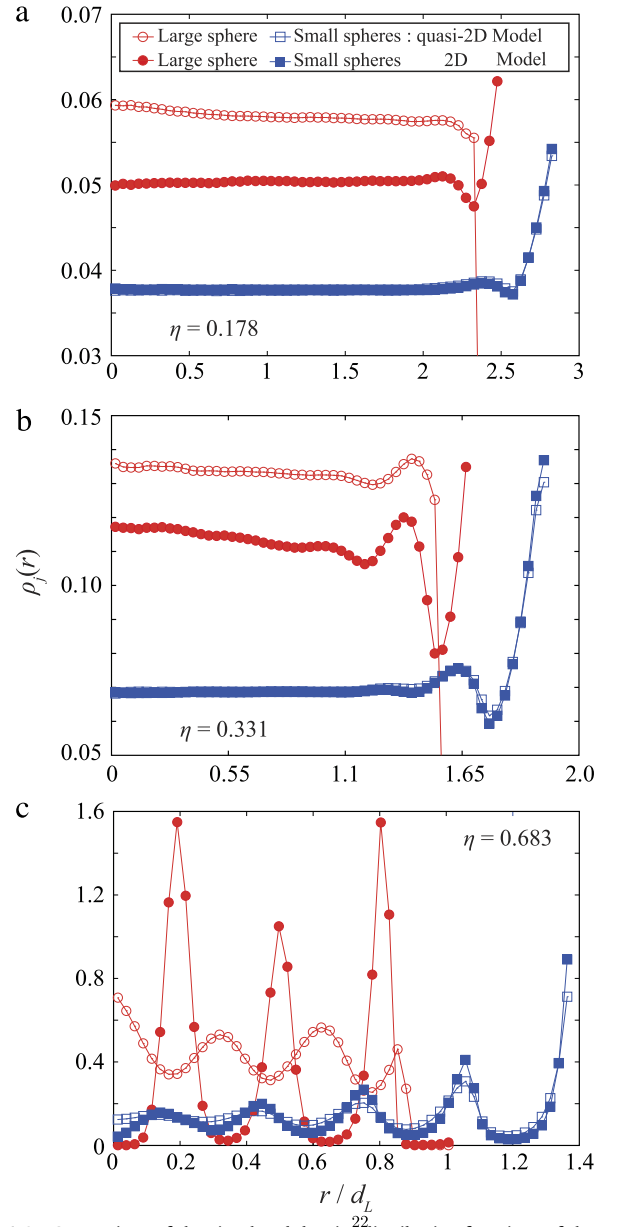


Fig. A.1. Comparison of the simulated density distribution functions of the two-dimensional liquid (solid symbols) with that of the quasi-two-dimensional liquid (open symbols) for the large sphere (circles) and a small sphere (squares), in which the spatial fluctuation along the z -direction is incorporated, vertical to the surface, for different packing fractions $\eta = 0.178$ in (a), 0.331 in (b) and 0.683 in (c). Lines are for eye guide.

liquid, denoted by open symbols for the large sphere (circles) and a small sphere (squares), in which the spatial fluctuation along the z -direction is incorporated (vertical to the surface) for different packing fractions $\eta = 0.178$ in (a), 0.331 in (b) and 0.683 in (c). In Fig. A.1(a), under the z -direction fluctuation, corresponding to its direct contact with the wall, diminishes compared to that of the two-dimensional model. In the quasi-2D model, the depletion force that drives the large sphere to the cavity wall is now compromised by this extra degree of freedom of spheres due to the fluctuation along the z -direction. Also, the large sphere distributes preferentially in the interior of the cavity in the quasi-2D model, whereas the probability of finding the large sphere near the cavity wall in the 2D model. As the packing fraction is increased to $\eta = 0.33$ in Fig. A.1(b), both models now show similar density profiles, that is, the large sphere is preferentially localized near both the cavity wall and the central region of the cavity. In the highest density

case of Fig. A.1(c), the large sphere in both models is excluded from the cavity wall. Its density distribution function shows pronounced liquid-like order with oscillatory pattern depending on the chosen model, indicating that the extra degree freedom along z -direction induces different local packing between the large sphere and small spheres. Nevertheless, the fact that the large and small spheres tightly pack in the highly dense mixture remains valid. For small spheres, the density distribution function for both models shows insignificant difference at all packing fractions, and small spheres pack from the cavity wall towards the inner region.

In the quasi-2D model, the z -direction fluctuation is responsible for diminishing the density distribution of the large sphere at near the cavity wall due to the higher local density of small spheres around the cavity boundary. As a result, it promotes the large sphere shifting towards the interior of the cavity, by which the chance of the large sphere to overlap with small spheres can be reduced (Note that the number of small spheres near center is the lowest.) This result is consistent with our observation in Fig. 2. Through the qualitative comparison of the experimentally determined density distribution function (i) in Fig. 2(b), it shows that at the low packing fraction in Fig. A.1(a), the large sphere in the quasi-2D model has a fair probability distributing around the cavity wall, and shows the feature similar to that of the 2D model except near the area in direct contact with wall. By increasing the packing fraction to the case in Fig. A.1(b), both models show that the large sphere distribute near the wall and the central region of the cavity with similar probability as in (ii) of Fig. 2(b). At the highest packing fraction as in Fig. A.1(c), the large sphere in the quasi-2D model displays the behavior that resembles the experiment observation with less pronounced oscillation in $\rho_L(r)$ and a near steady increase towards the center of the cavity in (iii) of Fig. 2(b). These findings indicate that in the real experiment, the spatial fluctuation due to vibration is different from the simulation model and is roughly between the 2D and the quasi-2D model. Moreover, Monte Carlo simulation deals with equilibrium systems without energy dissipation. Such a method may not provide the entire picture of our non-equilibrium experiment. Nevertheless, the simulation models render the opportunity to clarify the possible role of the spatial fluctuation introduced by the vibration in experiment.

Appendix B. Supplementary material

Supplementary material related to this article can be found online at <http://dx.doi.org/10.1016/j.physd.2016.06.014>.

References

- [1] K. Chen, J. Cole, C. Conger, J. Draskovic, M. Lohr, K. Klein, T. Scheidemantel, P. Schiffer, Granular materials: Packing grains by thermal cycling, *Nature* 442 (2006) 257.
- [2] G.C. Barker, Computer simulations of granular materials, in: A. Mehta (Ed.), *Granular Matter*, Springer, 1994.
- [3] S.B. Zimmerman, A.P. Minton, Macromolecular crowding: Biochemical, biophysical, and physiological consequences, *Annu. Rev. Biophys. Biomol. Struct.* 22 (1993) 27–65.
- [4] R.J. Ellis, Macromolecular crowding: an important but neglected aspect of the intracellular environment, *Curr. Opin. Struct. Biol.* 11 (2001) 114–119.
- [5] K. Richter, M. Nesslering, P. Lichter, Macromolecular crowding and its potential impact on nuclear function, *Biochim. Biophys. Acta* 1783 (2008) 2100–2107.
- [6] S. Asakura, F. Oosawa, On interaction between two bodies immersed in a solution of macromolecules, *J. Chem. Phys.* 22 (1954) 1255–1256.
- [7] N.A. Denesyuk, D. Thirumalai, Entropic stabilization of the folded states of RNA due to macromolecular crowding, *Biophys. Rev.* 5 (2013) 225–232.
- [8] S. Schnell, T.E. Turner, Reaction kinetics in intracellular environments with macromolecular crowding: simulations and rate laws, *Prog. Biophys. Mol. Biol.* 85 (2004) 235–260.
- [9] R. Hancock, Packing of the polynucleosome chain in interphase chromosomes: evidence for a contribution of crowding and entropic forces, *Semin. Cell Dev. Biol.* 18 (2007) 668–675.
- [10] D. Miyoshi, N. Sugimoto, Molecular crowding effects on structure and stability of DNA, *Biochimie* 90 (2008) 1040–1051.
- [11] Y. Komatsu, H. Tanaka, Roles of energy dissipation in a liquid–solid transition of out-of-equilibrium, *Phys. Rev. X* 5 (2015) 031025.
- [12] F. Pacheco-Vazquez, F. Ludewig, S. Dorbolo, Dynamics of a grain-filled ball on a vibrating plate, *Phys. Rev. Lett.* 113 (2014) 118001.
- [13] A. Rosato, K.J. trandburg, F. Prinz, R.H. Swendsen, Why the Brazil nuts are on top: Size segregation of particulate matter by shaking, *Phys. Rev. Lett.* 58 (1987) 1038.
- [14] R. Jullien, P.A. Meakin, A mechanism for particle size segregation in three dimensions, *Nature* 344 (1990) 425–427.
- [15] I.S. Aranson, L.S. Tsimring, Patterns and collective behavior in granular media: Theoretical concepts, *Rev. Modern Phys.* 78 (2006) 641.
- [16] T. Schnautz, R. Brito, C.A. Kruehle, I.A. Rehberg, Horizontal brazil-nut effect and its reverse, *Phys. Rev. Lett.* 95 (2005) 028001.
- [17] N.I. Lebovka, Aggregation of charge colloidal particles, *Adv. Polym. Sci.* 255 (2014) 57–96.
- [18] C.-Y. Shew, K. Yoshikawa, A toy model for nucleus-sized crowding confinement, *J. Phys.: Condens. Matter* 27 (2015) 064118.